Design of a surface-emitting, subwavelength metal-clad disk laser in the visible spectrum

Jingqing Huang, Se-Heon Kim, and Axel Scherer

Department of Electrical Engineering, California Institute of Technology, Mail Code 200-36, Pasadena, CA 91125-3600, USA

jingqing@caltech.edu

Abstract: We analyze metal-clad disk cavities designed for nanolasers in the visible red spectrum with subwavelength device size and mode volume. Metal cladding suppresses radiation loss and supports low order modes with room temperature Q of 200 to 300. Non-degenerate single-mode operation with enhanced spontaneous emission coupling factor β is expected with the TE_{011} mode that has a $0.46(\lambda_0/n)^3$ mode volume and $Q = 210$ in a device of size $0.12\lambda_0^3$. Threshold gain calculations show that room temperature lasing is possible using multiple GaInP/AlGaInP quantum wells as the gain medium. Placing a planar metal reflector under the cavity can enhance radiation and extraction efficiencies or increase the Q, without incurring additional metallic absorption loss. We show that the far-field radiation characteristics are strongly affected by the devices' immediate surroundings, such as changes in metal cladding thickness, even as the resonant mode profile, frequency, and Q remain the same. When the metal cladding is 1 μm thick, light radiates upward with a distinct intensity maximum at 45°; when the cladding is 100 nm thick, the emitted light spreads in a near-horizontal direction.

OCIS codes: (140.3410) Laser resonators; (140.3945) Microcavities; (140.7300) Visible lasers; (230.5750) Resonators; (250.7270) Vertical emitting lasers; (260.3910) Metal optics.

References and links

1. D. A. B. Miller, "Device Requirements for Optical Interconnects to Silicon Chips," Proc. IEEE **97,** 1166–1185 (2009)
2. M. Lončar, A. Scherer, and Y. M. Qiu, "Photonic crystal laser sources for chemical detection," Appl. Phys. Lett. **82,** 4648–4650 (2003)
3. S.-H. Kim, J.-H. Choi, S.-K. Lee, S.-H. Kim, S.-M. Yang, Y.-H. Lee, C. Seessal, P. Regrency, and P. Viktorovitch, "Optofluidic integration of a photonic crystal nanolaser," Opt. Express **16,** 6515–6527 (2008)
4. S. Kita, K. Nozaki, and T. Baba, "Refractive index sensing utilizing a cw photonic crystal nanolaser and its array configuration," Opt. Express **16,** 8174–8180 (2008)
5. E. M. Purcell, "Spontaneous emission probabilities at radio frequencies," Phys. Rev. **69,** 681 (1946)
6. J.-M. Gérard and B. Gayral, "Strong Purcell effect for InAs quantum boxes in three-dimensional solid-state microcavities," J. Lightwave Technol. **17,** 2089–2095 (1999)
7. K. Nozaki, S. Kita, and T. Baba, "Room temperature continuous wave operation and controlled spontaneous emission in ultrasmall photonic crystal nanolaser," Opt. Express **15,** 7506–7514 (2007)
8. T. Yoshie, M. Lončar, A. Scherer, and Y. M. Qiu, "High frequency oscillation in photonic crystal nanolasers," Appl. Phys. Lett. **84,** 3543–3545 (2004)
9. H. Altug, D. Englund, and J. Vučković, "Ultrafast photonic crystal nanocavity laser," Nat. Phys. **2,** 484–488 (2006)

#132188 - $15.00 USD Received 23 Jul 2010; revised 21 Aug 2010; accepted 24 Aug 2010; published 31 Aug 2010

10. A. Mizrahi, V. Lomakin, B. A. Slutsky, M. P. Nezhad, L. Feng, and Y. Fainman, "Low threshold gain metal coated laser nanoresonators," Opt. Lett. **33,** 1261–1263 (2008)
11. Q. Song, H. Cao, S. T. Ho, and G. S. Solomon, "Near-IR subwavelength microdisk lasers," Appl. Phys. Lett. **94,** 061109 (2009)
12. K. Yu, A. Lakhani, and M. C. Wu, "Subwavelength metal-optic semiconductor nanopatch lasers," Opt. Express **18,** 8790–8799 (2010)
13. Y. Akahane, T. Asano, B.-S. Song, and S. Noda, "High-Q photonic nanocavity in a two-dimensional photonic crystal," Nature **425,** 944–947 (2003)
14. J. Scheuer, W. M. J. Green, G. A. DeRose, and A. Yariv, "Lasing from a circular Bragg nanocavity with an ultrasmall modal volume," Appl. Phys. Lett. **86,** 251101 (2005)
15. P. B. Deotare, M. W. McCutcheon, I. W. Frank, M. Khan, and M. Lončar, "High quality factor photonic crystal nanobeam cavities," Appl. Phys. Lett. **94** 121106 (2009)
16. P. B. Johnson and R. W. Christy, "Optical constants of the noble metals," Phys. Rev. B **6,** 4370 (1972)
17. D. W. Lynch and W. R. Hunter, "Comments on the optical constants of metals and an introduction to the data for several metals," in *Handbook of Optical Constants of Solids I,* E. D. Palik, eds. (Academic, San Diego, Calif., 1998), pp. 275–367.
18. J. A. Dionne, L. A. Sweatlock, and H. A. Atwater, "Plasmon slot waveguides: Towards chip-scale propagation with subwavelength-scale localization," Phys. Rev. B **73,** 035407 (2006)
19. H. T. Miyazaki and Y. Kurokawa, "Controlled plasmon resonance in closed metal/insulator/metal nanocavities," Appl. Phys. Lett. **89,** 211126 (2006)
20. A. Hosseini and Y. Massoud, "Nanoscale surface plasmon based resonator using rectangular geometry," Appl. Phys. Lett. **90,** 181102 (2007)
21. M. T. Hill, Y.-S. Oei, B. Smalbrugge, Y. Zhu, T. de Vries, P. J. van Veldhoven, F. W. M. van Otten, T. J. Eijkemans, J. P. Turkiewicz, H. de Waardt, E. J. Geluk, S.-H. Kwon, Y.-H. Lee, R. Nötzel, and M. K. Smit, "Lasing in metallic-coated nanocavities," Nat. Photon. **1,** 589–594 (2007)
22. J.-C. Weeber, A. Bouhelier, G. Colas des Francs, L. Markey, and A. Dereux, "Submicrometer in-plane integrated surface plasmon cavities," Nano Lett. **7,** 1352–1359 (2007)
23. M. P. Nezhad, A. Simic, O. Bondarenko, B. Slutsky, A. Mizrahi, L. Feng, V. Lomakin, and Y. Fainman, "Room-temperature subwavelength metallo-dielectric lasers," Nat. Photon. **4,** 395–399 (2010)
24. Y. Arakawa and H. Sakaki, "Multidimensional quantum well laser and temperature dependence of its threshold current," Appl. Phys. Lett. **40,** 939–941 (1982)
25. K. Inoshita and T. Baba, "Fabrication of GaInAsP/InP photonic crystal lasers by ICP etching and control of resonant mode in point and line composite defects," IEEE J. Sel. Top. Quantum Electron. **9,** 1347–1354 (2003)
26. A. Farjadpour, D. Roundy, A. Rodriguez, M. Ibanescu, P. Bermel, J. D. Joannopoulos, S. G. Johnson, and G. Burr, "Improving accuracy by subpixel smoothing in FDTD," Opt. Lett. **31,** 2972–2974 (2006)
27. V. A. Mandelshtam and H. S. Taylor, "Harmonic inversion of time signals," J. Chem. Phys. **107,** 6756–6769 (1997). Erratum, ibid. **109,** 4128 (1998).
28. A. Taflove and S. C. Hagness, *Computational Electrodynamics - The Finite-Difference Time-Domain Method* (Artech House, Norwood, 2005)
29. T. Baba, "Photonic crystals and microdisk cavities based on GaInAsP-InP system," IEEE J. Sel. Top. Quantum Electron. **3,** 808–830 (1997)
30. Z. Zhang, L. Yang, V. Liu, T. Hong, K. Vahala, and A. Scherer, "Visible submicron microdisk lasers," Appl. Phys. Lett. **90,** 111119 (2007)
31. C. E. Hofmann, E. J. R. Vesseur, L. A. Sweatlock, H. J. Lezec, F. J. G. de Abajo, A. Polman, and H. A. Atwater, "Plasmonic modes of annular nanoresonators imaged by spectrally resolved cathodoluminescence," Nano Lett. **7,** 3612–3617 (2007)
32. S.-W. Chang and S. L. Chuang, "Normal modes for plasmonic nanolasers with dispersive and inhomogeneous media," Opt. Lett. **34,** 91–93 (2009)
33. S.-W. Chang and S. L. Chuang, "Fundamental formulation for plasmonic nanolasers," IEEE J. Quantum Electron. **45,** 1014–1023 (2009)
34. S.-W. Chang, T.-R. Lin, and S. L. Chuang, "Theory of plasmonic fabry-perot nanolasers," Opt. Express **18,** 15039–15053 (2010)
35. H. Kato, S. Adachi, H. Nakanishi, and K. Ohtsuka, "Optical properties of $(Al_xGa_{1-x})_{0.5}In_{0.5}P$ quaternary alloys," Jpn. J. Appl. Phys. **33,** 186–192 (1994)
36. W. W. Chow, P. M. Smowton, P. Blood, A. Girndt, F. Jahnke, and S. W. Koch, "Comparison of experimental and theoretical GaInP quantum well gain spectra," Appl. Phys. Lett. **71,** 157–159 (1997)
37. G. Hunziker, W. Knop, and C. Harder, "Gain measurement on one, two, and three strained GaInP quantum well laser diodes," IEEE Trans. Quantum Electron. **30,** 2235–2238 (1994)
38. M. T. Hill, M. Marell, E. S. P. Leong, B. Smalbrugge, Y. Zhu, M. Sun, P. J. van Veldhoven, E. J. Geluk, F. Karouta, Y.-S. Oei, R. N otzel, C.-Z. Ning, and M. K. Smit, "Lasing in metal-insulator-metal sub-wavelength plasmonic waveguides," Opt. Express **17,** 11107–11112 (2009)
39. E. F. Schubert. Y.-H. Wang, A. Y. Cho, L.-W. Tu, and G. J. Zydzik, "Resonant cavity light-emitting diode," Appl.

#132188 - $15.00 USD Received 23 Jul 2010; revised 21 Aug 2010; accepted 24 Aug 2010; published 31 Aug 2010

Phys. Lett. **60,** 921–923 (1992)
40. H. Benisty, H. D. Neve, and C. Weisbuch, "Impact of planar microcavity effects on light extraction—part i: basic concepts and analytical trends," IEEE J. Quantum Electron. **34,** 1612–1631 (1998)
41. S.-H. Kim, S.-K. Kim, and Y.-H. Lee, "Vertical beaming of wavelength-scale photonic crystal resonators," Phys. Rev. B **73,** 235117 (2006)
42. R. A. Matula, "Electrical resistivity of copper, gold, palladium, and silver," J. Phys. Chem. Ref. Data **8,** 1147–1298 (1979)
43. C. A. Balanis, *Advanced Engineering Electromagnetics* (Wiley, New York, 1989).

1. Introduction

Miniaturized solid state lasers are useful components for applications ranging from optical communication [1] to on-chip spectroscopy [2, 3, 4]. Desirable device characteristics include single mode lasing with low pump power, high speed direct modulation, high radiation efficiency, directional emission, and small footprint for dense on-chip integration. Lasers with small optical mode volume V_{eff} have the particular advantage of enhanced spontaneous emission—whose figure of merit is the Purcell factor $F_p \propto Q/V_{eff}$ [5, 6]—which helps reduce lasing threshold [7] and increases modulation speed [8, 9]. To this end, there has been much research effort to reduce the size of lasers to (sub)wavelength scale [10, 11, 12]. Photon confinement using periodic structures such as Bragg gratings and photonic crystals has received much attention due to their high cavity Q/V_{eff}. However, dielectric periodic structures necessarily require the device size to be several times the wavelength in one or more dimensions [7, 13, 14, 15]. Metal-optic and plasmonic cavities have recently been of particular interest. Due to their dispersive dielectric function $\varepsilon_{metal} = \varepsilon_R + i\varepsilon_I$ whose real part ε_R is negative in the near-infrared (NIR) and visible spectrum [16, 17], metals such as gold and silver can be used to overcome the diffraction limit and confine electromagnetic energy to volumes much smaller than is possible in purely dielectric systems [18, 19, 20]. Yet metals also present considerable optical loss that worsens as wavelength decreases from NIR to visible. As a result, most subwavelength metallic cavities have room temperature (RT) Q factors of below 100 and so can only lase in cryogenic temperatures [12, 21, 22]. Mizrahi, Nezhad, Fainman and colleagues have proposed and demonstrated higher Q metallic cavities by inserting a low index silicon dioxide SiO_2 layer around the semiconductor gain material, that is thick enough to push the optical mode away from the metal [10, 23]. However, this complicates the realization of an electrically pumped laser based on the same design and preclude the use of metal as an effective heat sink, a feature that is proving to be important for small volume semiconductor lasers [24, 25].

In this article, we present a design of surface-emitting, subwavelength metal-clad disk laser cavities that have a RT Q-factor of 200 to 300 at the visible red wavelength of $\lambda_0 \sim 670$ nm, making it possible to lase without the need for cryogenic cooling. Non-degenerate single mode operation can be achieved by shrinking device size, retaining only the TE_{011} mode, and thereby increase the spontaneous emission coupling factor β. The laser cavity's Q and radiation and extraction efficiencies can be tuned by placing a reflector directly under the device's bottom surface. The TE_{011} mode can have a Q of 230, a V_{eff} of $0.46(\lambda_0/n)^3 \sim 0.004\ \mu m^3$ with a 400×400 nm^2 footprint. Its radiation efficiency can be tuned to as high as > 0.5 and the surface emission extraction efficiency to 0.2. In Section 2, we use finite-difference time-domain (FDTD) simulation [26, 27, 28] to analyze the disk cavities' relative loss mechanisms, namely material absorption and radiation loss, and evaluate spontaneous emission enhancement, radiation efficiency, and the threshold gain to assess the possibility of room temperature lasing. The control of radiation loss and tuning of radiation and extraction efficiencies are studied in Section 3.1; far-field radiation pattern and emission directionality are presented in Section 3.2. We conclude our discussion in Section 4.

#132188 - $15.00 USD Received 23 Jul 2010; revised 21 Aug 2010; accepted 24 Aug 2010; published 31 Aug 2010

2. Subwavelength cavity Q and spontaneous emission control

Dielectric disk cavities have Q-factors limited by radial radiation loss, which imposes a lower limit of $d_0 \approx 0.7$–$0.8\lambda_0$ on device size [11, 29, 30], where d_0 is the dielectric disk diameter. We consider, specifically, a disk laser cavity designed for the more localized transverse electric-like TE_{mpq} modes (m, p, and q are the azimuthal, radial, and axial mode numbers, respectively) at $\lambda_0 = 670$ nm. It has a thickness of 210 nm and a dielectric constant $\varepsilon_{dielectric} = 11$. The cavity Q falls sharply as the disk diameter shrinks, and a resonant mode with $m < 3$ can hardly exist, as is evident in Fig. 1.

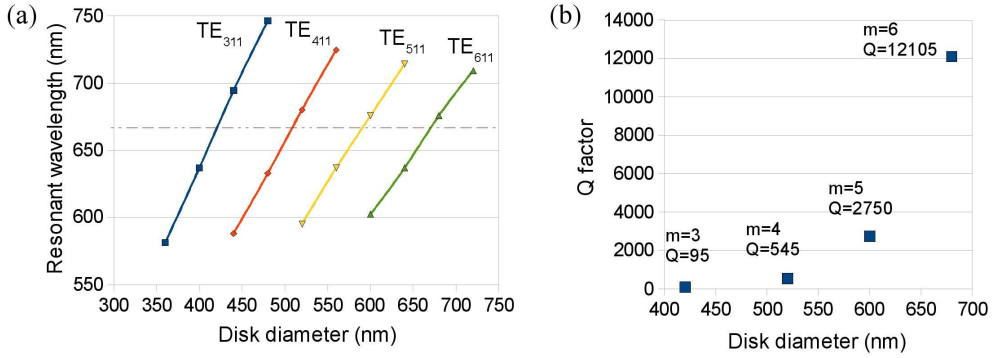

Fig. 1. (a) Resonant modes for various disk diameters, the dotted red line indicates $\lambda_0 = 670$ nm resonant wavelength; (b) Q-factors for various disk diameters at $\lambda_0 \approx 670$ nm: $d_0 = 210$ nm gives TE_{311} with $\lambda_0 = 667$ nm and $Q = 95$, $d_0 = 260$ nm gives TE_{411} with $\lambda_0 = 682$ nm and $Q = 545$, $d_0 = 300$ nm gives TE_{511} with $\lambda_0 = 677$ nm and $Q = 2750$, and $d_0 = 340$ nm gives TE_{611} with $\lambda_0 = 675$ nm and $Q = 12105$.

The metal-clad disk cavity studied in this article is shown schematically in Fig. 2(a). The semiconductor disk's curved surface is enclosed in an optically thick, reflective, and low loss metal layer. We choose to use silver, a relatively low loss metal in the visible spectrum, whose dispersive dielectric function can be described by fitting experimental data to the Drude model [16, 17, 31]

$$\varepsilon_{Ag}(\omega) = \varepsilon_h - \frac{(\varepsilon_s - \varepsilon_h)\omega_p^2}{\omega^2 + i\omega\gamma} \tag{1}$$

where, at room temperature, $\varepsilon_s = 6.18$ is the relative permittivity in the static limit, $\varepsilon_h = 5.45$ is the relative permittivity in the high frequency limit, $\omega_p = 1.72 \times 10^{16}$ rad/s is the plasma frequency, and $\gamma = 8.35 \times 10^{13}$ rad/s is the damping frequency. The skin depth of silver at this wavelength is about 25 nm, so a metal thickness of ≥ 100 nm in the radial direction is sufficient. We use a high resolution of 2 nm in the FDTD simulations to capture the rapid change of electromagnetic fields in metal. A subwavelength sized device with $d_0 = 420$ nm forms a multi-mode resonator and, due to the effective radiation loss inhibition by the silver cladding, supports the lowest order $m = 0, 1, 2, 3$ modes with Q-factors of 160 to 290; the non-degenerate $m = 0$ mode has a Q of 240. Normalized mode profiles are shown in Fig. 2(b)–(e). To obtain non-degenerate single mode operation, the device needs to be shrunk to $d_0 = 220$ nm, where only the TE_{011} mode is supported with a Q of 210; its mode profile is shown in Fig. 3(a)–(b). We note that the presence of silver cladding enables the co-existence of a $\lambda_0 \sim 670$ nm surface plasmon (SP) resonant mode, distinguished by its electric field maximum at the silver-dielectric interface, as shown in Fig. 3(c)–(d); however, it has a material absorption limited low

#132188 - $15.00 USD Received 23 Jul 2010; revised 21 Aug 2010; accepted 24 Aug 2010; published 31 Aug 2010

Q of about 50, since a large fraction of the electromagnetic field exists in the metal cladding and suffers much ohmic loss.

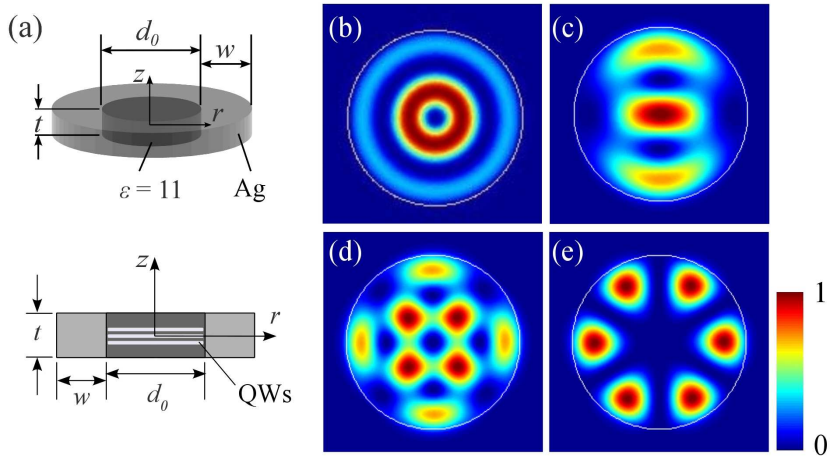

Fig. 2. (a) 3D schematic and sideview cross-section of the silver-clad disk cavity, the origin of the coordinate system is located at the center of the dielectric disk; (b)–(e) Electric-field intensity distribution $|\mathbf{E}|^2$ of resonant modes in a $d_0 = 420$ nm cavity: $m = 0$ (TE_{021}, $\lambda_0 = 642$ nm, $Q = 240$), $m = 1$ (TE_{122}, $\lambda_0 = 660$ nm, $Q = 160$), $m = 2$ (TE_{221}, $\lambda_0 = 676$ nm, $Q = 230$), and $m = 3$ (TE_{311}, $\lambda_0 = 675$ nm, $Q = 290$), respectively. Field maximum is at $z = 0$ for $m = 0, 2, 3$ and at $z \approx \pm t/4$ for $m = 1$. White circle indicates the dielectric-silver interface.

Optical cavities with subwavelength physical size and mode volume utilize a metal that has a large negative ε_R at the desired resonant frequency to suppress radiation loss [10, 12, 21, 23, 38]; however, the metal also presents significant absorption loss. The two loss channels' relative contribution to device Q is given by $Q_{tot}^{-1} = Q_{rad}^{-1} + Q_{abs}^{-1}$, where Q_{tot} is the total device Q, Q_{rad} and Q_{abs} are the Q-factors due to radiation and material absorption loss, respectively. The radiation loss also represents the signal we can collect from the laser, we can thus define a device radiative efficiency η_{rad} as the ratio of power loss due to radiation alone P_{rad} over the total power loss P_{tot}:

$$\eta_{rad} \equiv \frac{P_{rad}}{P_{tot}} = \frac{1/Q_{rad}}{1/Q_{tot}} \tag{2}$$

Moreover, the extent of spontaneous emission enhancement is an important characteristic of (sub)microscale lasers. We calculate the Purcell factor for the metal-clad disk lasers using [6]

$$F_p = \frac{3Q(\lambda_0/n)^3}{4\pi^2 V_{eff}} \tag{3}$$

where V_{eff} is given by [32, 33]

$$V_{eff} = \frac{\int_V (\frac{\partial(\omega\varepsilon)}{\partial\omega} + \varepsilon_R)|\mathbf{E}|^2 dV}{\max[(\frac{\partial(\omega\varepsilon)}{\partial\omega} + \varepsilon_R)|\mathbf{E}|^2]}. \tag{4}$$

To evaluate if the cavity can lase, the threshold material gain g_{th} is determined by [33, 34]

$$g_{th} = \frac{\omega_0}{Q v_{g,a}(\omega_0)\Gamma_E} \tag{5}$$

#132188 - $15.00 USD Received 23 Jul 2010; revised 21 Aug 2010; accepted 24 Aug 2010; published 31 Aug 2010

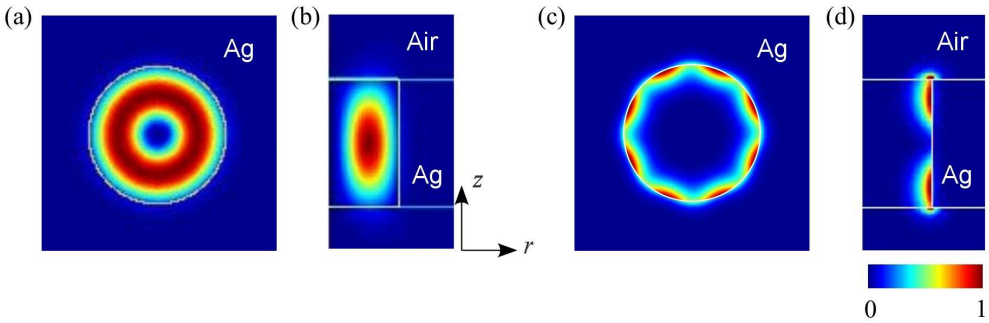

Fig. 3. Electric-field intensity distribution $|\mathbf{E}|^2$ of modes in a $d_0 = 220$ nm cavity: TE_{011} mode at (a) the horizontal center plane $z = 0$ and (b) the vertical center plane of the disk, $\lambda_0 = 663$ nm; surface plasmon (SP) mode at (c) the horizontal $z = 80$ nm plane and (d) the vertical center plane through field intensity maxima, $\lambda_{SP} = 675$ nm. White lines indicate material interfaces.

where ω_0 is the resonant frequency and $v_{g,a}(\omega_0) \approx c/n_{g,a}(\omega_0)$ is the material group velocity. Γ_E is the energy confinement factor

$$\Gamma_E = \frac{\int_{Va} \frac{\varepsilon_0}{4}\{\varepsilon_{g,a}(\omega_0) + \Re[\varepsilon_a(\omega_0)]\}|\mathbf{E}|^2 dV}{\int_V \frac{\varepsilon_0}{4}\{\varepsilon_g(\mathbf{r}), \omega_0) + \Re[\varepsilon(\mathbf{r}, \omega_0)]\}|\mathbf{E}|^2 dV} \tag{6}$$

in which $\varepsilon_g = \frac{\partial}{\partial \omega}\Re[\omega\varepsilon(\mathbf{r}, \omega)]$ and subscript a denotes active gain material. We use experimentally measured and fitted dielectric function $\varepsilon_a(\omega)$ for GaInP/AlGaInP [35], the semiconductor commonly used as the active material for visible red spectrum, and assume that optical gain comes from 7 or 9 7-nm thick GaInP quantum wells (QWs) separated by 10-nm thick $Al_{0.3}GaInP$ barriers [30, 36] with the middle well located at the $z = 0$ plane, as shown in Fig. 2(a). g_{th} per well can then be approximated by g_{th}/N, where N is the number of quantum wells [37].

Table 1. Comparative characteristics of metal-clad disk modes

	d_0 = 220 nm		d_0 = 420 nm			
	$m = 0$	SP mode	$m = 0$	$m = 1$	$m = 2$	$m = 3$
Q_{tot}	210	54	240	160	230	290
λ_0 [nm]	663	664	642	660	676	675
V_{eff} $[(\lambda_0/n)^3]$	0.46	0.23	0.71	0.80	1.27	1.36
F_p	35	18	26	15	14	16
η_{rad}	0.16	0.00017	0.47	0.72	0.39	0.33
Γ_E (7 QWs)	0.34	0.14	0.32	0.17	0.34	0.14
g_{th} per QW [cm^{-1}]	846	7691	801	2288	764	1487
Γ_E (9 QWs)	0.39	0.24	0.38	0.27	0.39	0.21
g_{th} per QW [cm^{-1}]	565	3544	537	1090	516	759

The calculated results are given in Table 1. For comparison, we include data for the aforementioned SP resonant mode. The $m = 0$ modes experience the most spontaneous emission enhancement due to their relatively high Q, smaller V_{eff}, and non-degeneracy. All of the low order non-plasmonic resonant modes have similar or better Purcell factor and much better radiation efficiency compared with the SP mode. The SP mode's low Q and poorer Γ_E also results

#132188 - $15.00 USD Received 23 Jul 2010; revised 21 Aug 2010; accepted 24 Aug 2010; published 31 Aug 2010

in much higher g_{th}, making RT lasing unlikely. The $m = 0, 2$ modes have g_{th} per QW of 764–846 cm^{-1} with 7 QWs. With 9 QWs, the non-plasmonic modes' g_{th} per well ranges between 516–1090 cm^{-1}, corresponding to threshold carrier densities of 3.5–4.8 $\times 10^{18}$ cm^{-3}, which are achievable in GaInP/AlGaInP at room temperature [36, 37].

3. Tuning radiation characteristics

3.1. Radiation efficiency

Directional emission is a desired laser characteristic; it enables efficient collection of the emitted light. A metal-clad disk laser such as one shown in Fig. 2(a) evidently radiates through both its top and bottom surfaces. It is difficult to collect light in both directions; half of the radiated light would be lost. We can thus think of placing a reflector under the disk to redirect the downward traveling light, as has been proposed for microcavity LEDs [39, 40] and photonic crystal resonators [41]. To keep to the subwavelength size and mode volume and to be able to place the reflector arbitrarily close to the resonator's bottom surface, we use an optically thick silver layer instead of Bragg reflectors. A silicon dioxide SiO_2 spacer of thickness h is used to tune the radiation characteristics. Other low index materials can also be used for better thermal conductivity, such as silicon nitride or aluminum oxide. The device structure is shown in Fig. 4(a). To illustrate the effect of the bottom reflector, we study the non-degenerate TE_{011} mode (see Fig. 3). The electric field has its maximum located at $z = 0$ and decays to small magnitude at the $\varepsilon = 11$ dielectric disk's top and bottom surfaces. Silver has a large negative real dielectric constant $\varepsilon_R \approx -22$ at $\lambda_0 = 670$ nm [16, 17]. Therefore, the bottom reflector results in little change in the resonant mode profile, even when it is in contact with the disk resonator, as shown in Fig. 4(b).

Although we are mostly interested in (near-)RT operation for laser applications, it is nevertheless instructive to look at the effect of the bottom reflector at lower temperatures. The low temperature metallic dielectric function $\varepsilon_{Ag}(\omega)$ can be estimated using the resistivity versus temperature $\rho_{Ag}(T)$ data of silver [42]. The damping frequency is proportional to material resistivity, and is 1% and 18% of its RT value at $T = 30$ K and 80 K, respectively. The total and component Q-factors and the radiation efficiency η_{rad}—defined in Eq. 2—as a function of the SiO_2 spacer thickness h are plotted in Figs. 2(c)–(e), using the same scale for all temperatures. For comparison, Q_{rad} and η_{rad} for metal-clad disk cavities suspended in air or on a SiO_2 substrate ($h = \infty$) without the bottom reflector are also indicated in the figures.

Loss due to metallic absorption does not change much, regardless of the presence of the bottom silver reflector or its position. Q_{abs} is consistently about 250 at RT, 1400 at 80 K, and a couple of tens of thousands at 30 K. The increase in Q_{abs} with respect to temperature is as expected, due to the corresponding decrease in resistivity and thus ohmic loss in silver. On the other hand, Q_{rad} and η_{rad} are strongly modulated by the bottom reflector. By varying the spacer thickness h, Q_{rad} changes between 225 and 2710, and thereby enhances or deteriorates Q_{tot}.When $h \leq 150$ nm, Q_{rad} is enhanced with no additional material absorption loss, consequently at RT Q_{tot} is increased to 230, from $Q_{tot} = 150$ for a laser cavity on SiO_2 substrate or $Q_{tot} = 210$ for one suspended in air with no bottom reflector. When $h \approx 250$ nm, however, Q_{rad} is at a minimum and Q_{tot} deteriorates to 120. η_{rad} is also tuned by varying h, from 0.08 (when Q_{rad} is at a maximum of 2710 with $h = 80$ nm) to 0.52 (when Q_{rad} is at its minimum of 225 with $h = 270$ nm). The same trend is seen in cryogenic temperatures, even as Q_{tot} changes from material absorption limited at RT to radiation loss limited at 30 K.

For many applications, the emitted light would be collected or interfaced to other devices via the metal-clad disk's top surface. This calls for a new figure of merit, extraction efficiency η_{extr}, which is the ratio of collectible radiation power loss from the laser cavity over total power loss. For a surface emitting laser, η_{extr} is the ratio of power loss due to radiation through

#132188 - $15.00 USD Received 23 Jul 2010; revised 21 Aug 2010; accepted 24 Aug 2010; published 31 Aug 2010

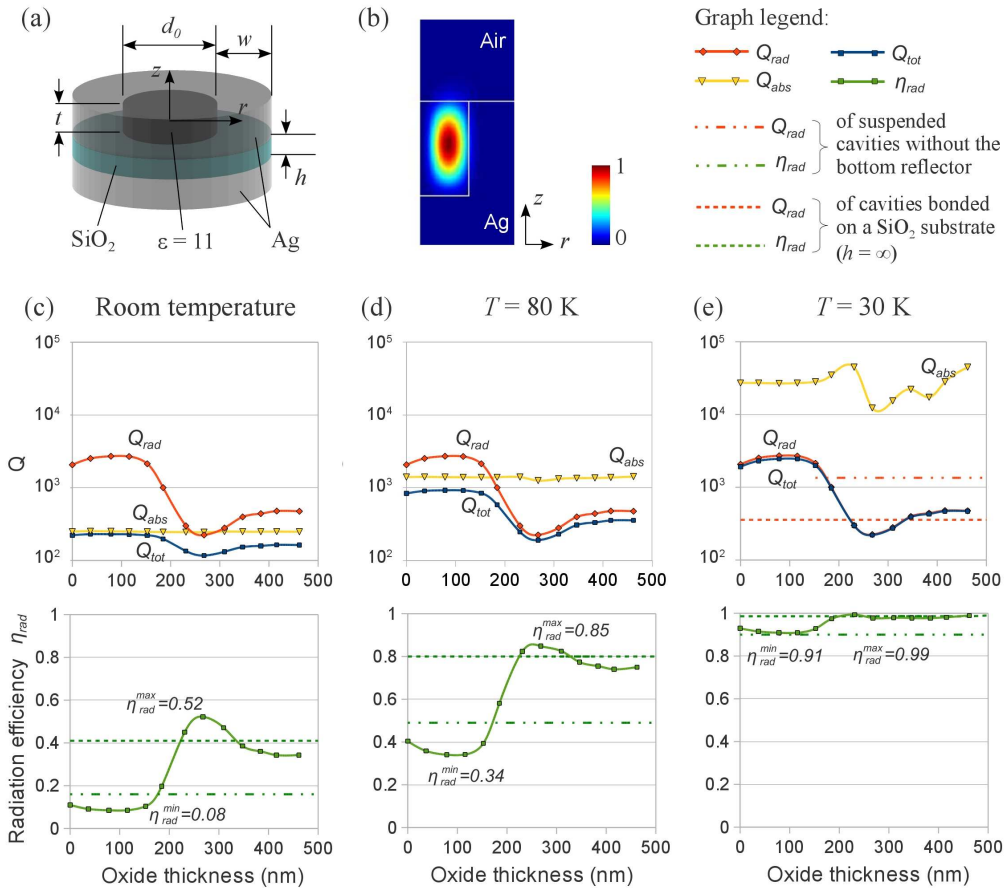

Fig. 4. Effect of the bottom reflector on radiation characteristics: (a) Schematic of device structure, the origin of the coordinate system is located at the center of the $\varepsilon = 11$ dielectric disk; (b) electric-field intensity distribution $|\mathbf{E}|^2$ of the TE_{011} mode in a $d_0 = 220$ nm resonator with a Ag bottom reflector and $h = 0$; Q-factor decomposition (Q_{tot}, Q_{rad}, and Q_{abs}) and η_{rad} for different oxide thicknesses h at (c) room temperature, (d) 80 K, and (e) 30 K, plotted on the same scale for comparison. Upper and lower dotted orange lines indicate Q_{rad} for a suspended metal-clad disk laser and for one on a SiO_2 substrate, respectively, both without a bottom reflector. Upper and lower dotted green lines indicate η_{rad} for a metal-clad disk laser on SiO_2 substrate and for one suspended in air, respectively.

#132188 - $15.00 USD Received 23 Jul 2010; revised 21 Aug 2010; accepted 24 Aug 2010; published 31 Aug 2010

the cavity's top surface over total power loss. η_{extr} of a suspended metal-clad laser resonator without a bottom reflector is simply a half of its total radiation efficiency $\frac{1}{2}\eta_{rad}$. The presence of the spacer raises the concern of possible loss of emitted light in the radial direction in the spacer layer, since it effectively forms a $Ag/SiO_2/Ag$ slab waveguide. We perform an energy flux calculation to determine the extent of this effect and the laser's η_{extr} for various h. With a spacer thickness of $h \leq 210$ nm, $> 99\%$ of the radiated power are directed upward through the laser disk's top surface, giving $\eta_{extr} \approx \eta_{rad}$. This is because the cavity mode couples effectively to the transverse-electric (TE, $E_z = 0, H_z \neq 0$) slab waveguide modes, but not the transverse-magnetic (TM) and surface plasmon (SP) modes. The TE modes are cut off for $h \leq 210$ nm; light only couples to the free-space radiation modes through the top surface. When $h > 210$ nm, over 75% of the radiated light couples to the TE mode in the spacer, surface emission extraction efficiency η_{extr} suffers. In the range of $0 < h < 210nm$, η_{extr} is equal to or greater than that of the suspended laser cavity with no bottom reflector for all temperatures: at RT η_{extr} =0.08–0.32 compared with 0.08 without the reflector, 0.34–0.70 compared with 0.24 at 80 K, and 0.91–0.97 compared with 0.49 at 30 K.

3.2. Far-field radiation pattern

We proceed to study the far-field radiation pattern of the surface-emitting metal-clad disk laser. Using the surface equivalence theorem [41, 43] and the numerical methods described in [28, 41], we set up the calculation geometry as shown in Fig. 5(a). The far-field electric field intensity $|\mathbf{E}_{tot}|^2$ on the hemisphere $S_\cap$ and its θ- and φ-polarized components $|E_\theta|^2$ and $|E_\varphi|^2$ (direction of θ and φ are shown in the calculation geometry) are determined by the tangential field components E_r, E_φ, H_r, and H_φ on the surface $S_{||}$. Normalized far-field intensities in $S_\cap$ are plotted in Fig. 5(b) and (c) with the laser surface normal at the center, and 30°, 60°, and 90° from surface normal are indicated with dotted white circles.

First, to study the far-field radiation pattern due to light emission from the top surface alone, we extend the cladding thickness w to 1 μm in order to block any interference due to light emitted from the disk's bottom surface and reflected off material interfaces. The TE_{011} mode from a $d_0 = 220$ nm cavity exhibits a mostly φ-polarized far-field radiation with negligible θ-polarization, which is analogous to the far-field pattern of the monopole mode in a single-defect photonic crystal cavity [41]. The radiation is directed upward, with the field intensity maximum at about 45° from surface normal, as shown in Fig. 5(b). We find that the far-field pattern remains unchanged with or without the bottom reflector and as we vary the spacer thickness h.

As we reduce w, however, we find that the radiated light interact with the laser cavity's surroundings; the far-field pattern is strongly affected. Take the example of the TE_{011} mode with a bottom reflector and $h = 0$, where the only light emission is through the laser cavity's top surface. Varying w from 1 μm to 100 nm, the resonator retains its resonant wavelength of $\lambda_0 = 660.2$ nm and a Q_{tot} of 210 to 226. The far-field radiation remains φ-polarized, but its field intensity distribution changes from having a distinct maximum at 45° to spreading in the horizontal direction between 60° and 90°; the device changes from a surface-emitting laser to a horizontal emitter with poorer directionality, as is evident in Fig. 5(c). Thus in designing subwavelength lasers, one needs to be aware of the influence on the directionality of the emitted light by structures surrounding the laser cavity. While a metal cladding thickness of several times the metal's skin depth is sufficient to suppress radiation loss and create a laser resonator, it may need to be of wavelength scale to obtain light emission in the desired direction.

#132188 - $15.00 USD Received 23 Jul 2010; revised 21 Aug 2010; accepted 24 Aug 2010; published 31 Aug 2010

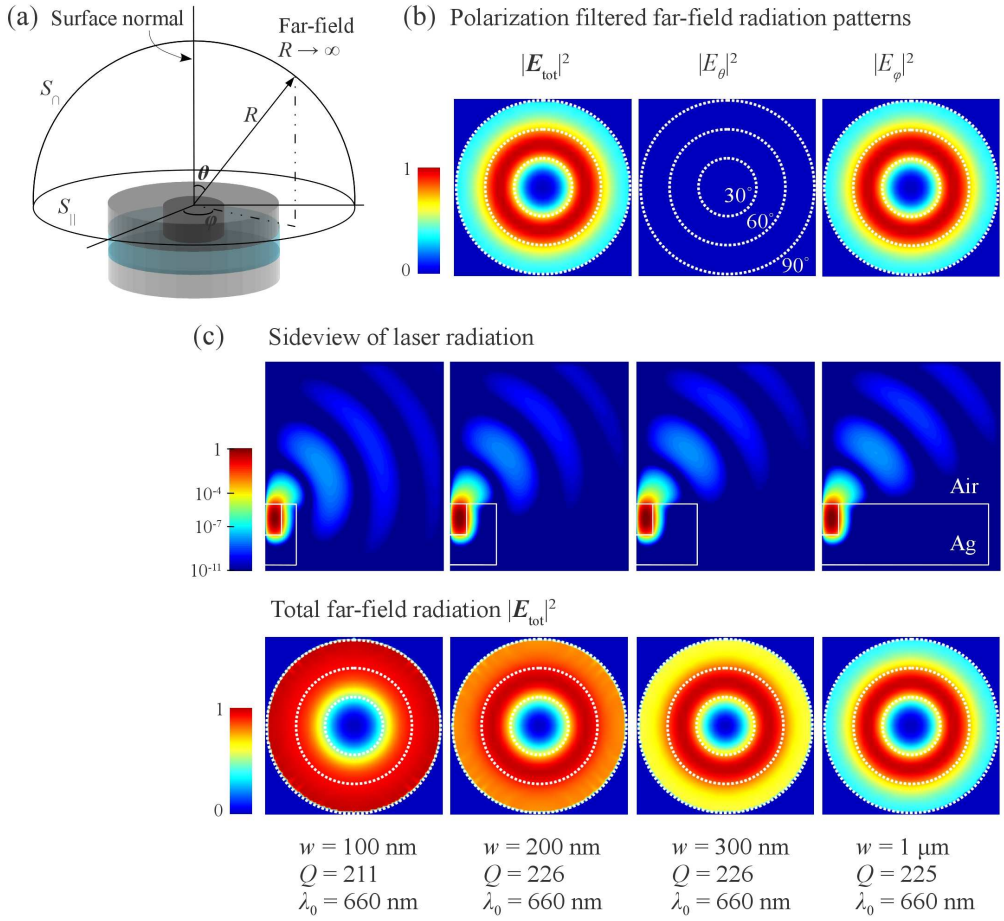

Fig. 5. (a) Geometry used to calculate far-field radiation patterns. The infinite hemispherical domain is located just above the laser cavity's top surface. Far-field radiation pattern is calculated on the dome in the limit of $R \to \infty$. Polarization directions θ and φ are shown. (b) Total and polarization filtered far-field radiation patterns, $|\mathbf{E}_{tot}|^2$, $|E_\theta|^2$, and $|E_\varphi|^2$, of the TE_{011} mode in a $d_0 = 220$ nm laser cavity. (c) Laser radiation sideview and the corresponding total far-field radiation patterns of the TE_{011} mode in $d_0 = 220$ nm metal-clad disk cavities with different Ag cladding thicknesses $w = 100$ nm, 200nm, 300nm, and 1 μm. White lines in radiation sideviews denotes material interface. Dotted white circles on far-field radiation patterns denote 30°, 60°, 90° from surface normal.

#132188 - $15.00 USD Received 23 Jul 2010; revised 21 Aug 2010; accepted 24 Aug 2010; published 31 Aug 2010

4. Conclusion

We have designed a disk laser cavity with subwavelength physical and effective mode volumes, by using metal-cladding to suppress radiation loss and thus increase the Q-factors of the low order $m = 0, 1, 2, 3$ modes. Non-degenerate single mode operation can be obtained with the TE_{011} mode, enhancing the spontaneous emission coupling factor β. Energy confinement factor Γ_E and threshold gain g_{th} calculations show that room temperature lasing is possible using 7 to 9 GaInP/AlGaInP quantum wells as the gain medium.

We can increase the laser's vertical radiation coupling or enhance its Q by placing a bottom reflector under the resonator. In doing so, we have quite a tuning range for these radiation characteristics while keeping the device's physical dimensions smaller than λ_0^3. For a mode that has its intensity maximum at $z = 0$ in a semiconductor slab of thickness $\geq (\lambda_0/n)$, a metallic bottom reflector can be brought to close proximity or in contact with the dielectric cavity to tune laser radiation and Q without incurring extra material loss. We expect similar techniques can be used to control the radiation of micro- and nanoscale laser cavities of other geometries.

We show that subwavelength metal-clad lasers' directional emission is strongly influenced by structures in the cavity's immediate surrounding, such as the cladding thickness, even as the laser's resonant wavelength and Q remain the same. This property needs to be taken into account when designing isolated lasers with directional emission or a coupled laser array.

The metal-clad disk laser resonators can sustain reasonable Q-factors while the dielectric disk is in contact with silver on all but the top surface; thus, they have a very effective heat sink and allow much freedom in designing electrical contact for current-injection operation. For example, the dielectric disk can be designed to have a vertical p-i-n doping profile. Top and bottom electrical contact can be established using silver or ITO. A thin electrical insulator, such as 10 nm thick silicon nitride, will need to be inserted, so the appropriate electrical path is established while light confinement using silver cladding is maintained. Alternatively, a radial doping profile can be used. For the $m \neq 1$ modes, which have zero electric field intensity at $r = 0$, we can place one electrode at the center of the disk's top surface and use the silver cladding around the curved surface as the other contact, while electrically insulating the disk from the bottom silver reflector. The design proposed in this article presents useful devices for applications that require small, densely integrated on-chip light source, such as telecommunication and lab-on-chip spectroscopy.

Acknowledgement

The authors would like to acknowledge support from the Defense Advanced Research Projects Agency under the Nanoscale Architecture for Coherent Hyperoptical Sources programme under grant #W911NF-07-1-0277 and from the National Science Foundation through NSF CIAN ERC under grant #EEC-0812072.

#132188 - $15.00 USD Received 23 Jul 2010; revised 21 Aug 2010; accepted 24 Aug 2010; published 31 Aug 2010